

## Tailward leap of multiple expansions of the plasma sheet during a moderately intense substorm: THEMIS observations

Yonghui Ma,<sup>1,2</sup> Chao Shen,<sup>1</sup> V. Angelopoulos,<sup>3</sup> A. T. Y. Lui,<sup>4</sup> Xinlin Li,<sup>5</sup> H. U. Frey,<sup>6</sup> M. Dunlop,<sup>7</sup> H. U. Auster,<sup>8</sup> J. P. McFadden,<sup>6</sup> and D. Larson<sup>6</sup>

Received 28 March 2012; revised 4 June 2012; accepted 6 June 2012; published 26 July 2012.

[1] A moderately intense substorm on 1 March 2008, from 0830 to 1000 UT, observed by THEMIS probes and the Ground Based Observatory (GBO) is examined to investigate the global evolution of substorm phenomena. During this interval, all five THEMIS probes are closely aligned along the tail axis near midnight covering a radial range from  $\sim 9$  Re to  $\sim 18$  Re. After the substorm onset, plasma sheet expansions take place successively at multiple locations in the magnetotail as measured by different probes. The positions of the plasma sheet expansions have a tailward leap progression with an average velocity of  $\sim 36$  km/s. There are two types of dipolarization detected in this substorm. The first type is the dipolarization front which is associated with the bursty bulk flow (BBF). While the second type, which we call ‘global dipolarization’, is associated with plasma sheet expansions. In the substorm studied, there are four intensifications as shown in the THEMIS AE index. We can detect the effects of localized and short-lived magnetic energy release processes occurring in the magnetotail corresponding to each of the four AE intensifications. Furthermore, the inner four probes can detect the global dipolarization signatures  $\sim 4$ – $15$  min earlier than plasma sheet expansions, while the outermost probe (P1) cannot detect this before the plasma sheet expansion. These two phenomena are caused by the same process (magnetic energy release process) but the effects detected by probes locally appear delayed. The observations in this case are not sufficient to distinguish between the two competing substorm models.

**Citation:** Ma, Y., C. Shen, V. Angelopoulos, A. T. Y. Lui, X. Li, H. U. Frey, M. Dunlop, H. U. Auster, J. P. McFadden, and D. Larson (2012), Tailward leap of multiple expansions of the plasma sheet during a moderately intense substorm: THEMIS observations, *J. Geophys. Res.*, *117*, A07219, doi:10.1029/2012JA017768.

### 1. Introduction

[2] Magnetospheric substorms are processes of the Earth’s magnetosphere responding to the variations in the solar wind, particularly the interplanetary magnetic field (IMF) [Akasofu, 1977]. Substorms are also crucial for energy

transport, coupling, and dissipation in the magnetosphere [Dungey, 1961; Akasofu, 1981; Gonzalez, 1990; Baker et al., 1996; Lu et al., 1998; Shen et al., 2002].

[3] The triggering mechanism of the onset of the expansion phase of substorms is a major controversial issue in magnetospheric physics. Two major internally triggering substorm models, the “near-Earth neutral line” (NENL) model [Hones et al., 1984; McPherron, 1991; Baker et al., 1996; Baumjohann, 2002; Angelopoulos et al., 2008b, 2009] and the “near-Earth current disruption” (NECD) model [Lui, 1996, 2009], describe most observational phenomena of substorms. According to the NENL model, magnetic reconnection  $\sim 20$  Re downstream in the mid-tail produces bursty bulk flows (BBFs) [Angelopoulos et al., 1992]; the BBFs transport energy earthward and are stopped at  $\sim -13$  to  $-15$  Re [Shiokawa et al., 1997]; Magnetic flux piles up, causing reduction of the cross-tail current, which leads to substorm current wedges (SCW) [Baker et al., 1996; Shiokawa et al., 1997, 1998; Birn et al., 1999]. On the other hand, according to the NECD model, instabilities in the near-Earth magnetotail lead to current disruption (CD), forming SCW and causing auroral breakup, thus to initiate substorm expansion [Lui et al., 1992; Lui, 1996]. And further, the rarefaction wave generated by the CD propagates tailward, eventually

<sup>1</sup>State Key Laboratory of Space Weather, Center for Space Science and Applied Research, Chinese Academy of Sciences, Beijing, China.

<sup>2</sup>College of Earth Science, Graduate University of Chinese Academy of Sciences, Beijing, China.

<sup>3</sup>Institute of Geophysics and Planetary Physics, University of California, Los Angeles, USA.

<sup>4</sup>Applied Physics Laboratory, Johns Hopkins University, Laurel, Maryland, USA.

<sup>5</sup>LASP and Department of Aerospace Engineering Sciences, University of Colorado Boulder, Boulder, Colorado, USA.

<sup>6</sup>Space Sciences Laboratory, University of California, Berkeley, California, USA.

<sup>7</sup>Rutherford Appleton Laboratory, Didcot, UK.

<sup>8</sup>IGEP, Technical University of Braunschweig, Braunschweig, Germany.

Corresponding author: Y. Ma, State Key Laboratory of Space Weather, Center for Space Science and Applied Research, Chinese Academy of Sciences, Beijing 100190, China. (yhma@spaceweather.ac.cn)

©2012. American Geophysical Union. All Rights Reserved.  
0148-0227/12/2012JA017768

causing magnetic reconnection and producing BBFs in the mid-tail [Lui *et al.*, 1992; Lui, 1996]. These two models are called ‘outside-in (NENL)’ and ‘inside-out (NECD)’, respectively. Another model, the global synthesis model, combines magnetic reconnection and current disruption [Pu *et al.*, 1999, 2001].

[4] Although the triggering mechanism for substorm expansion onset is still debated, the NENL and NECD models have a common feature, i.e., tailward retreat of global dipolarization in the magnetotail. Jacquey *et al.* [1991] and Ohtani *et al.* [1992] have first observed the outward progression of current disruption, although they claimed that it may prove that substorm onset occurs in the near-earth plasma sheet. Jacquey *et al.* [1991] have estimated the expansion velocity being  $\sim 300$  km/s and Ohtani *et al.* [1992] have estimated it  $\sim 200$  km/s. Baumjohann *et al.* [1999] have used a superposed epoch approach to study the substorm dipolarization at different radial distances. They have concluded that the dipolarization moves tailward at an average velocity of 35 km/s although they preferred the NENL model. Now it is known that the tailward retreat of the global dipolarization is a common phenomenon of the substorm expansion process.

[5] Lyons [1995, 1996] and Lyons *et al.* [1997] proposed that substorms may be triggered by certain solar wind processes that cause the reduction in the large-scale electric field. Their theory implies that, the northward turnings of the IMF Bz, decreases in the amplitude of the IMF By, and dynamic solar wind pressure changes may trigger substorms. Hsu and McPherron [2003] have shown that about 60% of substorms are triggered by IMF or solar wind dynamic pressure perturbations. Of those, about 10% are apparently associated with reduction in IMF |By| and no change in Bz, and about 3% appear to be triggered by dynamic pressure without either Bz or By changes. So 47% of substorms appear to be triggered by a northward turning of IMF Bz. Therefore, externally triggered substorms are also important in substorm research.

[6] During substorms, energy created from solar wind-magnetosphere coupling is first stored in the magnetotail and then dissipated in the magnetotail, inner magnetosphere and ionosphere [Akasofu, 1977; McPherron, 1979]. Sergeev *et al.* [1996] have argued that, two basic magnetospheric processes cause energy storage and dissipation in the magnetotail during substorm and non-substorm times. One is the slow and quasi-static global tail reconfiguration responsible for the energy storage, and the other are the local, sporadic, short-term energy dissipation events. The balance of these processes determines the type of the tail dynamic evolution. This coupled-mode scenario could be compatible with both the NENL model and NECD model in some extent [Sergeev *et al.*, 1996].

[7] The Time History of Events and Macroscale Interactions during Substorms (THEMIS) mission has been designed to have five probes (P5 (tha), P4 (the), P3 (thd), P2 (thc), and P1 (thb)) aligned along the tail axis with geocentric distances being about 10–30 Re so as to determine the origin of the substorm onset [Angelopoulos, 2008; Angelopoulos *et al.*, 2008a]. The THEMIS mission also has complementary ground-station observations for auroral activities and geomagnetic field variations [Donovan *et al.*, 2006; Mende *et al.*,

2008; Russell *et al.*, 2008]. The primary aim of THEMIS is to identify when and where substorms begin by examining the direction of substorm disturbance propagation in the magnetotail with five probes, and by examining auroral brightening to establish the global evolution of substorms. With the data from the five THEMIS probes and ground-station observations, many results on global evolution of substorms have been published [e.g., Runov *et al.*, 2008; Lui *et al.*, 2007, 2008; Angelopoulos *et al.*, 2008b].

[8] In this research, we will illustrate one substorm case in which the discrete and impulsive energy dissipation events take place during the expansion phase. A sequence of tailward-retreating global magnetic dipolarizations and multiple plasma sheet expansions from  $\sim 9$  Re to  $\sim 18$  Re after substorm expansion onset is also clearly identified. During this substorm event, the five THEMIS probes are closely aligned along the tail axis. Furthermore, the THEMIS AE index is also available for investigating the corresponding evolution in the auroral ionosphere. This paper is organized as follows. Section 2 shows the relevant instruments on board THEMIS and the data used in this study. Section 3 demonstrates the THEMIS AE index, ground-based observations of aurora, and solar wind conditions during this substorm. The development of the substorm in the magnetotail as observed by THEMIS five spacecraft is presented in Section 4. Section 5 gives the analysis and discussions. Last, a summary is presented in Section 6.

## 2. Instrumentation and Data

[9] After being launched on 17 February 2007, the orbits of the five THEMIS probes gradually evolved into elliptical, near-equatorial ones with apogees  $\sim 11.8$  Re for the three inner probes, and  $\sim 19.6$  Re and  $\sim 31.6$  Re for the two outer probes. Orbital periods for the probes are about 1, 2, or 4 days, allowing magnetotail alignment conjunctions once every 4 days during the tail season [Frey *et al.*, 2008]. During one such conjunction, from 0830 UT to 1000 UT on 1 March 2008, all five probes were in the pre-midnight sector near the plasma sheet. The locations of the five THEMIS probes at 0900 UT on 1 March 2008 are shown in Figure 1.

[10] Each THEMIS probe contains a fluxgate magnetometer (FGM) [Auster *et al.*, 2008], a search-coil magnetometer (SCM) [Roux *et al.*, 2008], an electric field instrument (EFI) [Bonnell *et al.*, 2008], a solid state telescope (SST) [Angelopoulos, 2008], and an electrostatic analyzer (ESA) [McFadden *et al.*, 2008a, 2008b]. The FGM is capable of detecting magnetic field variations with amplitudes of 0.01 nT and with high time resolution (0.007812 s for fgh mode; 3 s for fgs mode). The SCM is used to identify the possible role of waves in substorm breakups and expansion phases. The EFI measures the ambient vector electric field. The SST is used to measure energetic ( $>30$  keV) ion and electron distribution functions. The ESA plasma instrument is designed to measure ion and electron distribution functions from a few eV up to 30 keV for electrons and up to 25 keV for ions. Magnetic field (3 s time resolution) and plasma parameter data from THEMIS probes are used in this paper. We also use auroral data from the THEMIS ground-based all-sky imager (ASI) [Harris *et al.*, 2008; Mende *et al.*, 2008] and the

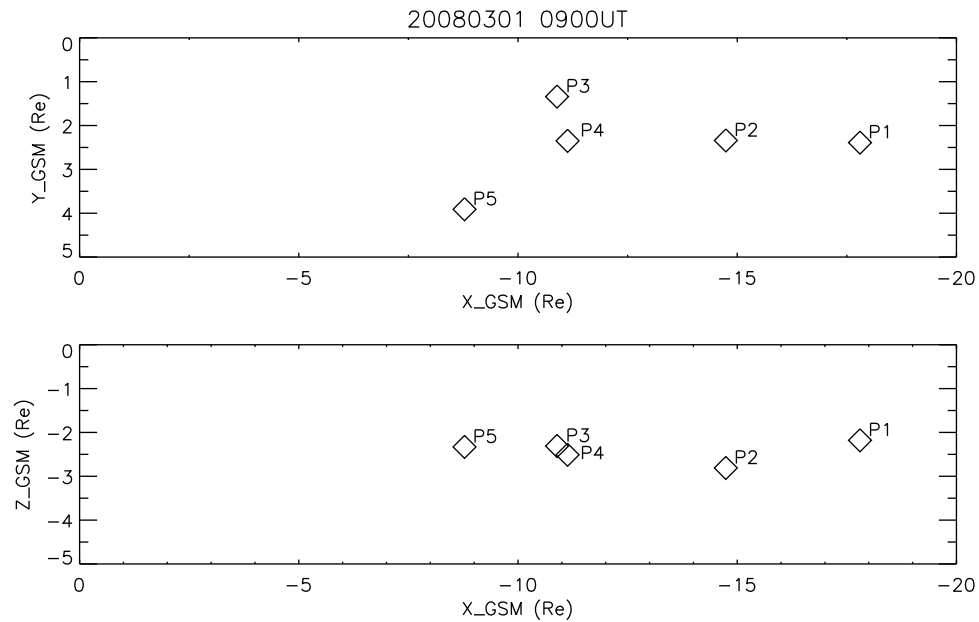


**Figure 1.** Locations of the five THEMIS probes in the  $X$ - $Y_{\text{GSM}}$  and  $X$ - $Z_{\text{GSM}}$  planes at 0900 UT on 1 March 2008.

THEMIS pseudo-AE index derived from THEMIS ground-based observatory (GBO) magnetometer data [Mende *et al.*, 2008; Russell *et al.*, 2008].

### 3. Ground-Based Observations and Solar Wind Conditions

#### 3.1. Auroral Electrojet

[11] The THEMIS pseudo-AE index during this major conjunction is shown in Figure 2. The maximum value of the

AE index is  $\sim 580$  nT at  $\sim 0907$  UT, indicating that it is a moderately intense substorm. The AE index during this substorm has four intensifications starting from  $\sim 0900:30$  UT,  $\sim 0908:30$  UT,  $\sim 0923:30$  UT, and  $\sim 0937$  UT respectively, as marked by four vertical dotted lines in Figure 2. The development of THEMIS pseudo-AE index implies that there are four intensifications during the auroral substorms. Furthermore, we may check the THEMIS spacecraft observations to see if the substorm activity in the magnetotail is also composed of discrete processes.

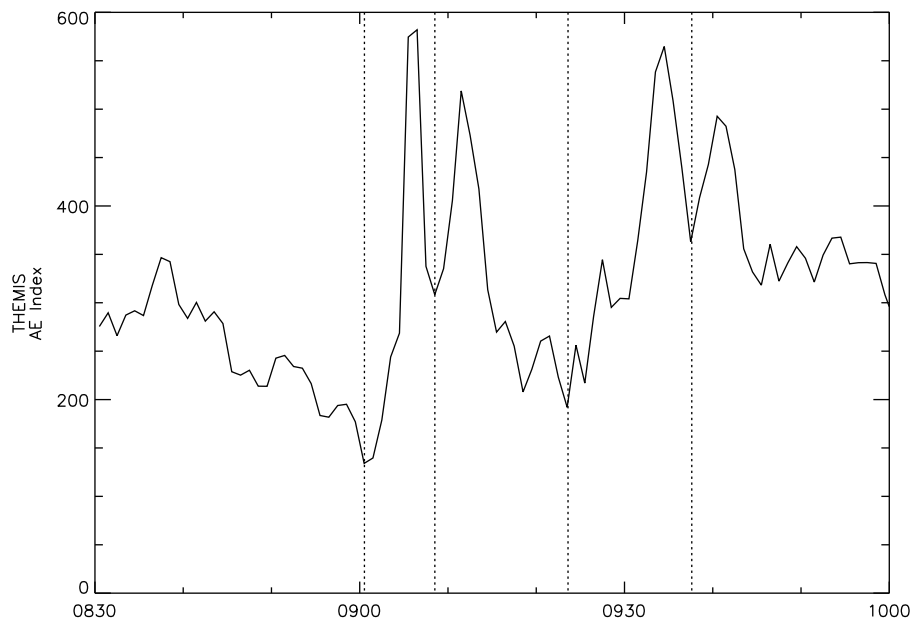


**Figure 2.** THEMIS pseudo-AE index during 0830 to 1000 UT on 1 March 2008. The four vertical lines show the beginning times of the four AE increases.

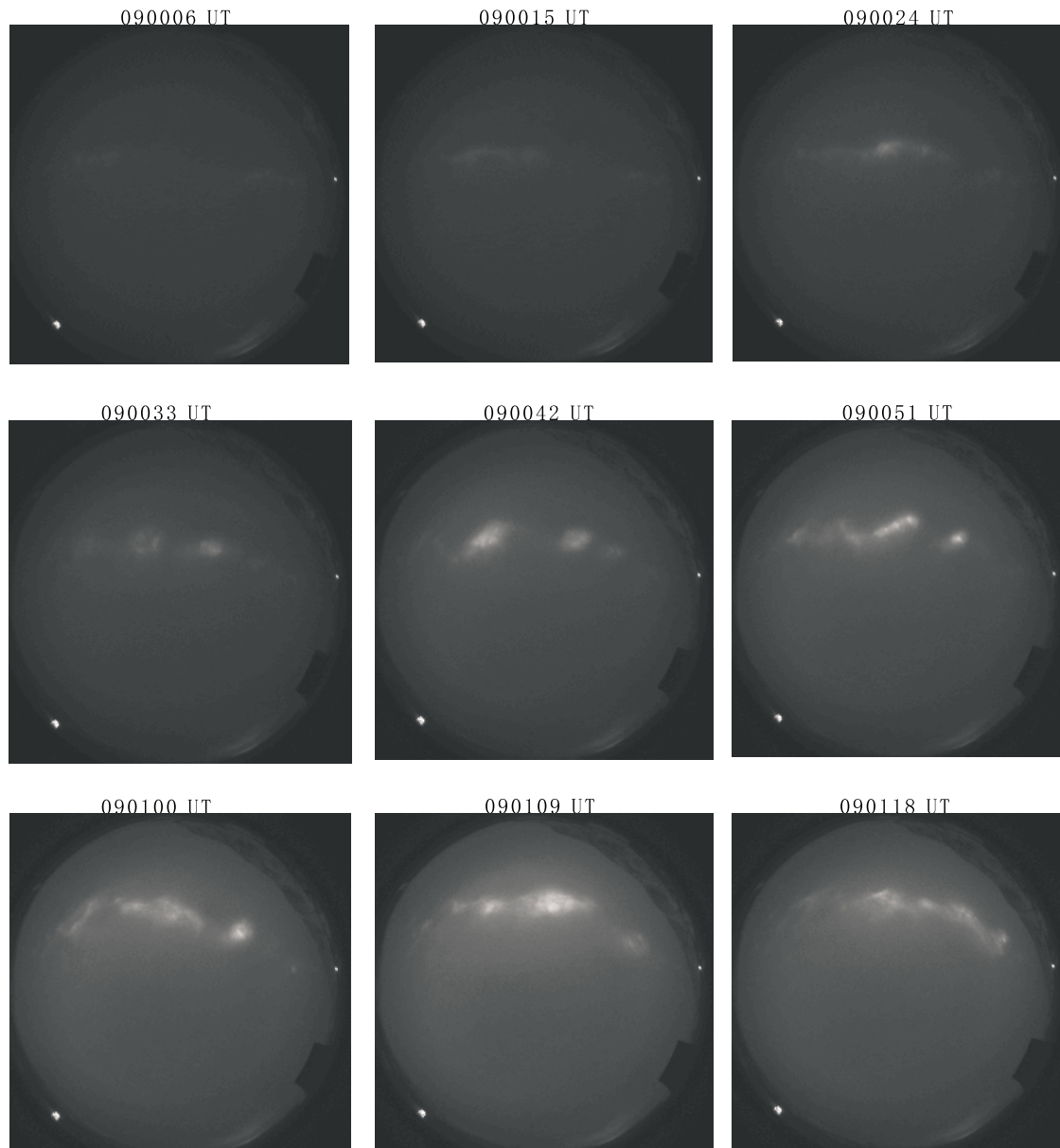


**Figure 3.** The time sequence of all sky images from White Horse (WHIT) during 0900:06 UT to 0901:18 UT on 1 March 2008. In the ASI auroral image, north is upward and east is to the right.

### 3.2. Auroral Development

[12] An important component of the THEMIS mission is the ground-based observatory (GBO) network of all-sky imagers (ASIs) [Mende *et al.*, 2008]. According to the T96 model [Tsyganenko, 1996], the footprints of the five THEMIS probes are (63.04N, 224.25E) for P5 (tha), (60.78N, 237.05E) for P4 (the), (61.67N, 233.70E) for P3 (thd), (62.18N, 236.16E) for P2 (thc), and (62.35N, 236.97E) for P1 (thb) in geographic coordinates at 0900 UT. P5 is located slightly to the west of WHIT (61.01N, 224.78E); P4, P3, P2, and P1 are between WHIT and FSIM (61.76N, 238.78E). Although the ASI data from FSIM are very poor due to cloud, onset is evident at WHIT, and it takes place exactly there. Figure 3 illustrates the evolution of auroral brightening from 0900:06 UT to 0901:18 UT (which contains the onset time of

this substorm) at WHIT on 1 March 2008, while Figure 4 shows the time series of integrated total image brightness from 0859 UT to 0901 UT at WHIT. From the ASI images (Figure 3) and the time series of total image brightness (the vertical dotted line in Figure 4), we can see clearly that the aurora brightens suddenly at 0900:15 UT. After that time, the aurora expands azimuthally and poleward. So this event is actually an auroral substorm. The onset time of auroral brightening (0900:15 UT) is very close to the beginning time of the first and largest increase in the THEMIS pseudo-AE index. So we may set 0900:15 UT as the onset time of this substorm.

### 3.3. Solar Wind Conditions

[13] To get the solar wind parameters at the location of magnetosphere, we have used the high-resolution OMNI

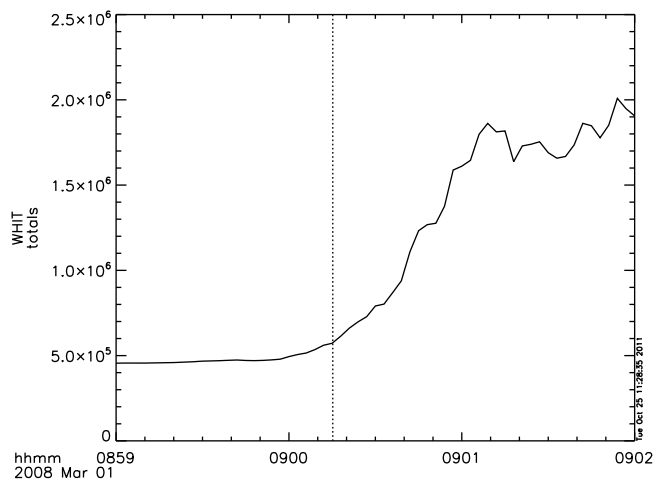


**Figure 4.** The integrated total brightness of all-sky camera images during 0859:00 UT to 0902:00 UT on 1 March 2008. The vertical line indicates the onset time of auroral breakup.

data deduced from the observation data of WIND satellite. WIND satellite is  $\sim 200$  Re upstream of the Earth's bow shock nose during this interval. The solar wind conditions are shown in Figure 5. The solar wind dynamic pressure is steady and has a value of  $\sim 1.2$ – $1.5$  nPa during this substorm, which could not be the triggering factor for substorm activity in the magnetotail. The interplanetary magnetic field (IMF)  $B_z$  (in GSM coordinates) turns to southward at  $\sim 0850$  UT and remains negative almost during the whole substorm except two short northward intervals. This means

that the dayside magnetic reconnection starts to occur prior to the substorm onset. The velocity of the solar wind is extremely strong and larger than 720 km/s during this substorm interval. So it is possible that the processes in the magnetotail are associated with the driving of the solar wind.

#### 4. Magnetotail Evolution During This Substorm

[14] In this section, we investigate the evolution of the substorm in the magnetotail based on the observations of THEMIS satellite. Simultaneous observations of the magnetic field and plasma parameters from P5, P3, P4, P2, and P1 are shown in Figures 6, 7, 8, 9, and 10, respectively. All the plasma moments and energy flux spectrum are computed after the cleaning of contamination from the sun (for the SST) and from the energetic electrons (for the ESA). For the electric field data, we use the data from EFI to get the  $E_x$  and  $E_y$  components in Despun SunSensor L-vectorZ (DSL) coordinate with  $E_z$  (equal to 0) along the spin axis. Then we subtract some reasonable offsets by looking at some quiet time earlier. Then we assume  $\mathbf{B} \cdot \mathbf{E} = 0$  to calculate  $E_z$  in DSL. To prevent the abnormally large and noisy  $E_z$  values, we restrict the ratio between  $B_z$  and the magnetic field component in the X-Y plane to be greater than  $\tan(5^\circ)$  [Liu *et al.*, 2011]. The  $E_z$  points with the magnetic field violating this criterion are set to be NaN values ( $E_x$  and  $E_y$  are also set to be NaN at these points), while the other points are rotated to GSM coordinates by using standard methods [Liu *et al.*, 2011]. The data gaps in  $E_{y\text{GSM}}$  are caused by this processing. For the calculation of the plasma pressure, ion density, ion velocity and ion temperature, we use the method discussed in the Appendix A of Saito *et al.* [2011].

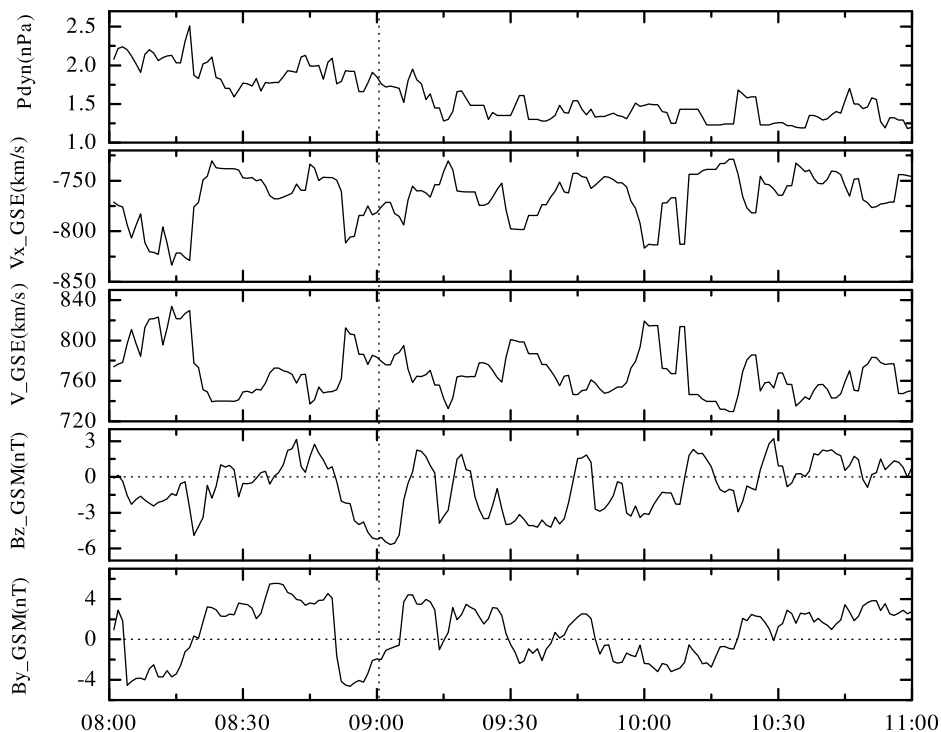


**Figure 5.** Solar wind conditions at the nose of the magnetopause from OMNI during the substorm on 1 March 2008. The black vertical dashed line indicates substorm onset time.

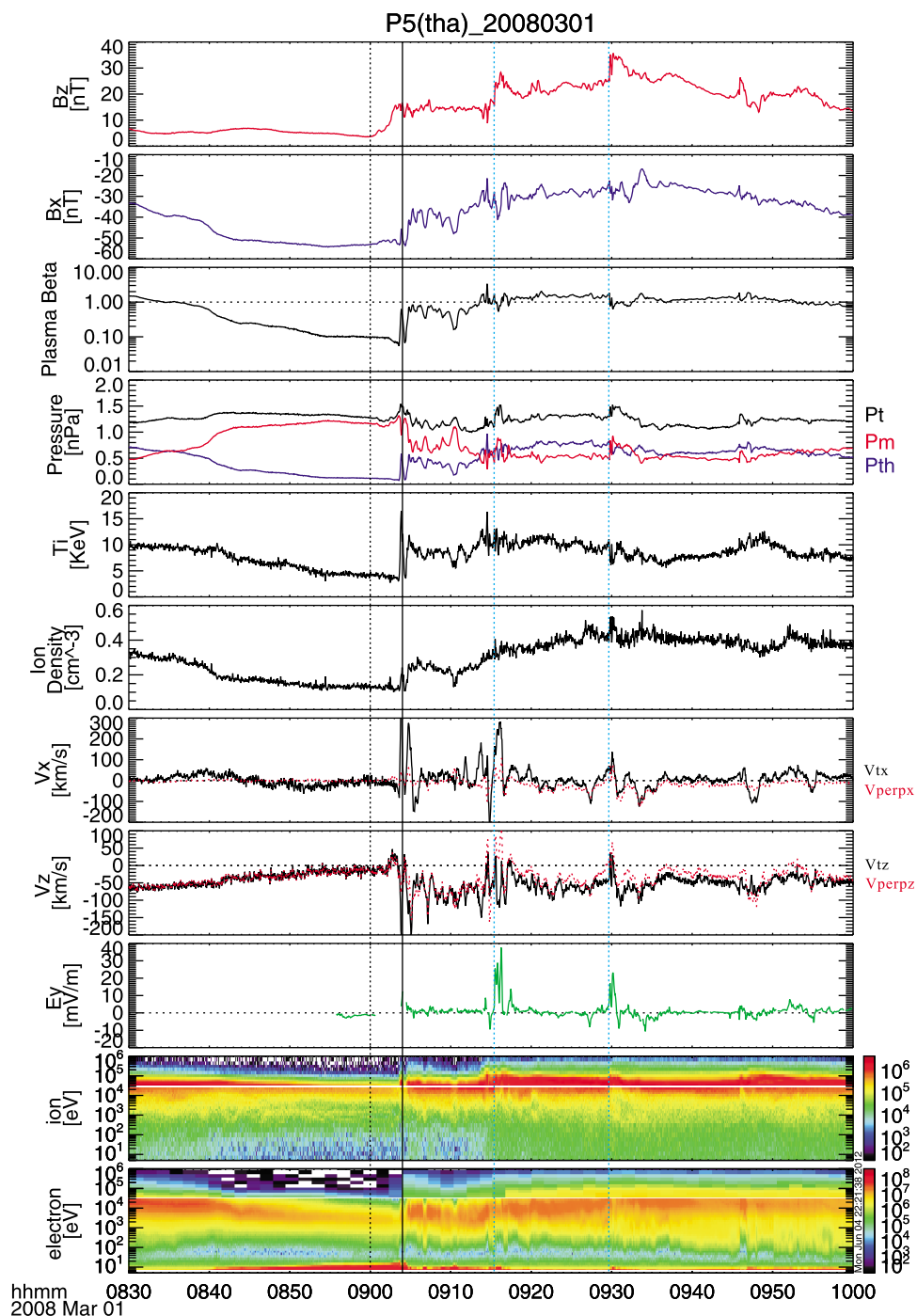


**Figure 6.** Variations of the magnetic field and plasma parameters as observed by P5 (tha) during 0830 to 1000 UT on 1 March 2008. Data from top to bottom panels: the Z component of magnetic field from FGM; the X component of magnetic field from FGM; the plasma beta (the ratio between the plasma pressure and the magnetic pressure); the plasma pressure (blue line), the magnetic pressure (red line) and total pressure (black line); the ion temperature; ion number density; the X component of the ion bulk velocity (black solid line) and perpendicular ion bulk velocity (red dotted line); the Z component of the ion bulk velocity (black solid line) and perpendicular ion bulk velocity (red dotted line); the Y component of the electric field; the ion energy flux spectrum from SST and ESA; and the electron energy flux spectrum from SST and ESA. Both the ion and electron energy flux spectrograms are in units of  $\text{eV}/(\text{cm}^2 \cdot \text{s} \cdot \text{sr} \cdot \text{eV})$ . The beta, pressures, temperature, velocity and density are all from combined ESA and SST. The velocity, magnetic field and electric field are in GSM coordinates. The black dotted vertical line, the black solid vertical line and the cyan dotted vertical line indicate the arrival time of the global dipolarization, the beginning time of plasma sheet expansion, and the beginning time of the dipolarization front, respectively.

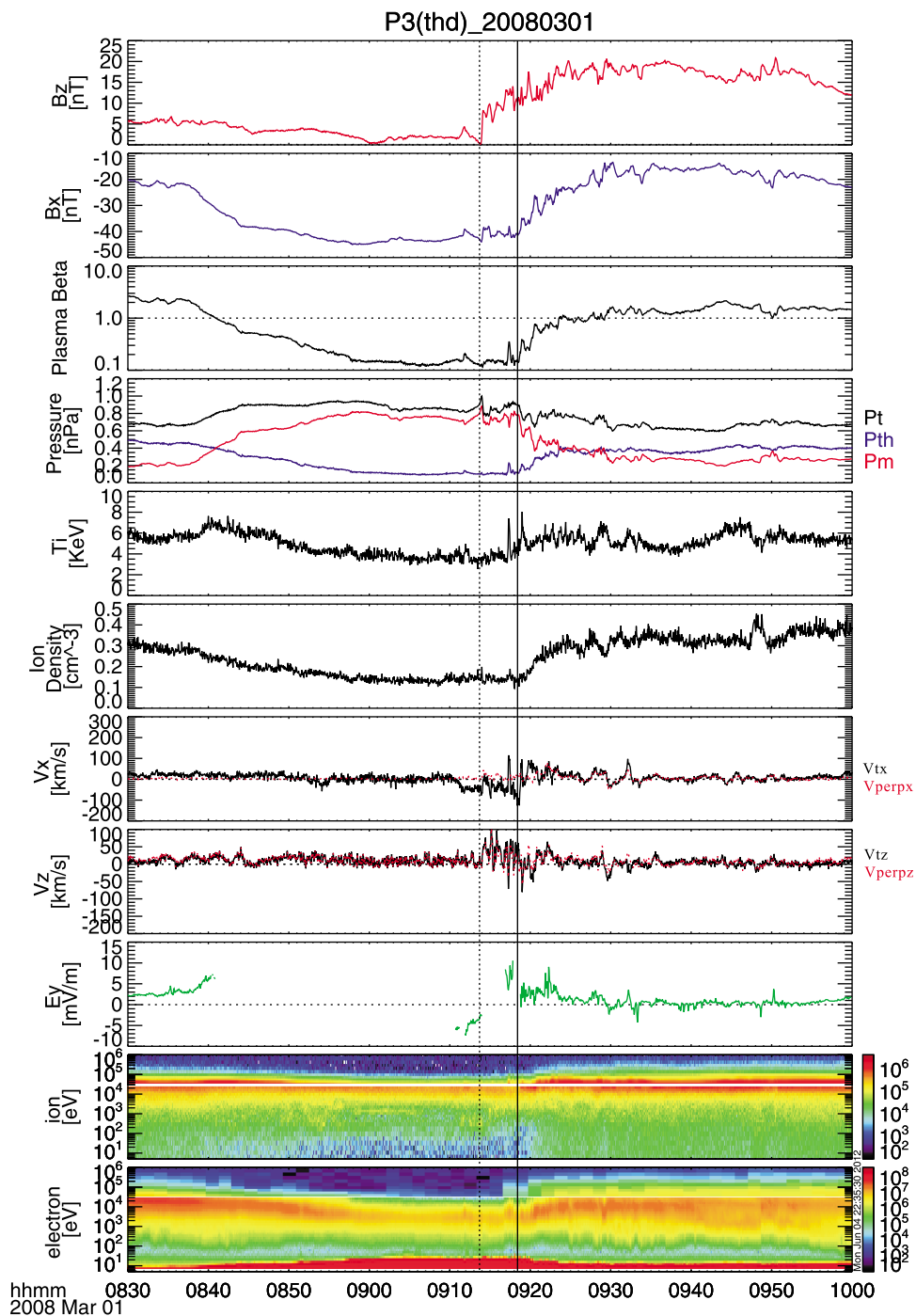


**Figure 7.** Variations of the magnetic field and plasma parameters as observed by P3 (thd) during 0830 to 1000 UT on 1 March 2008. Panel format is the same as that in Figure 6.

#### 4.1. Observations at THEMIS A (P5)

[15] An overview of P5 observations is shown in Figure 6. P5, the innermost THEMIS probe, is located at about  $(-8.78, 3.91, -2.33)$  Re in GSM coordinates at 0900 UT. As shown in the first panel of Figure 6, there are three magnetic dipolarization events having occurred.

[16] The first dipolarization event begins at  $\sim 0900$  UT (marked by the black vertical dotted line in Figure 6). P5 observes a clear increase in the Z component of magnetic

field ( $B_z$ ) (from  $\sim 5$  nT to  $\sim 15$  nT) starting at  $\sim 0900$  UT. At this time, as implied by the very low value ( $< 0.1$ ) of the plasma beta, P5 is located in the magnetotail plasma sheet boundary layer (PSBL) [Miyashita *et al.*, 2000]. The  $B_z$  increase indicates that the magnetic dipolarization arrival at P5. From  $\sim 0900$  UT to  $\sim 0904$  UT,  $B_z$  increases continuously and magnetic pressure ( $P_m$ ) increases slightly. As  $B_z$  is increasing during  $\sim 0900$  UT to  $\sim 0904$  UT, the energy flux spectrum of ions and electrons, ion velocity, ion density ( $N_i$ ), ion temperature ( $T_i$ ), plasma pressure ( $P_{th}$ ) and the X

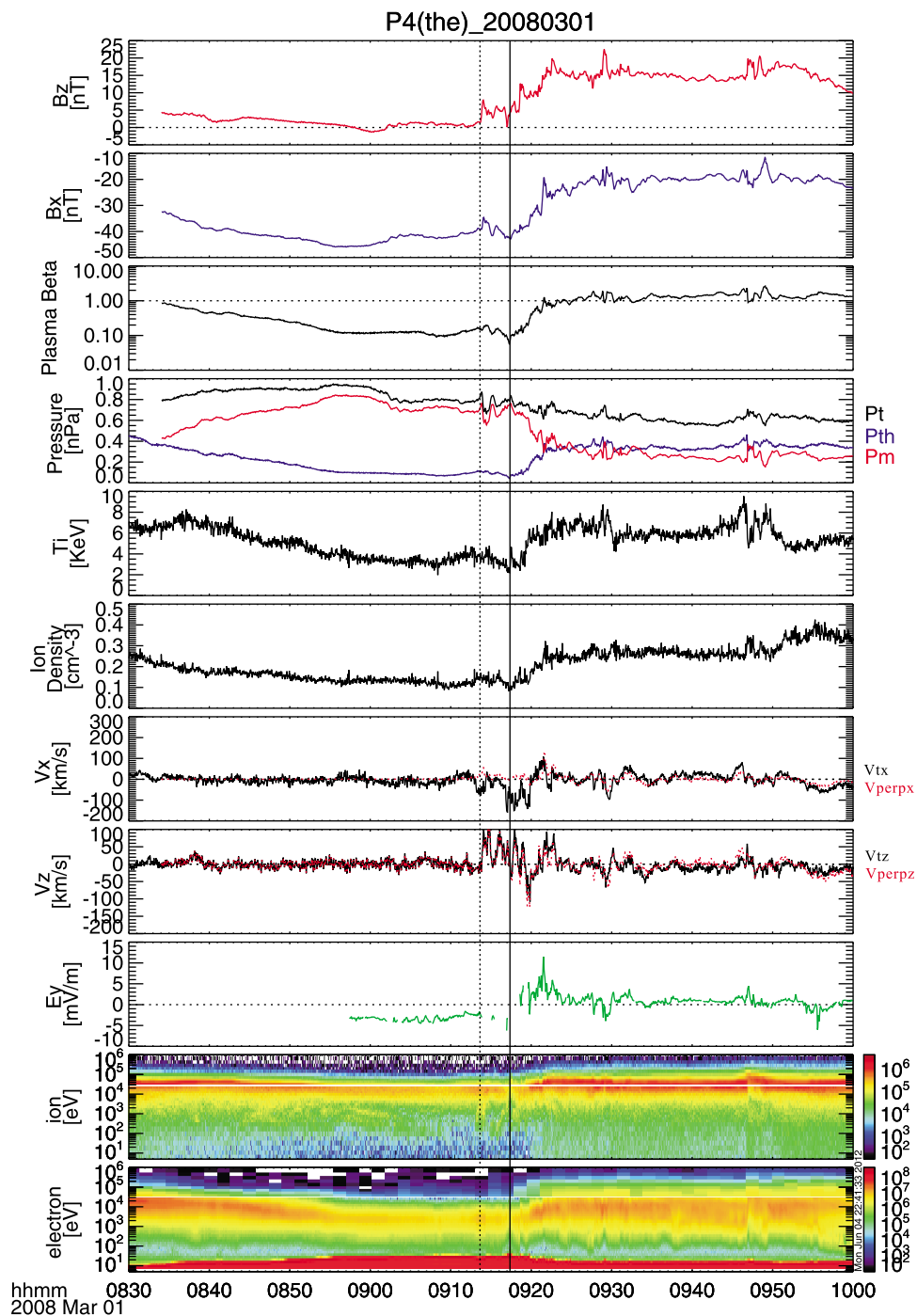


**Figure 8.** Variations of the magnetic field and plasma parameters as observed by P4 (the) during 0830 to 1000 UT on 1 March 2008. Panel format is the same as that in Figure 6.

component of magnetic field ( $B_x$ ) show no obvious variations. At  $\sim 0904$  UT (marked by the black vertical solid line in Figure 6), the absolute value of the X component of magnetic field ( $|B_x|$ ) begins to decrease suddenly, and the magnetic pressure ( $P_m$ ) and the total pressure ( $P_t$ ) drop sharply simultaneously. Meanwhile, the ion density ( $N_i$ ), ion temperature ( $T_i$ ) and plasma pressure ( $P_{th}$ ) have all increased considerably. The plasma (ion and electron) energy flux spectrum also begins to increase at  $\sim 0904$  UT. At the same time, the plasma beta suddenly jumps from less

than 0.1 to about 0.5. All these observations imply that P5 is penetrating into the plasma sheet since  $\sim 0904$  UT. At  $\sim 0910:30$  UT, some similar signatures as that at 0904 UT have been detected and the plasma beta increases to larger than 1. The Y component of electric field ( $E_y$ ) has a positive value and the Z component of perpendicular ion bulk velocity ( $V_{perpz}$ ) and ion bulk velocity ( $V_{tz}$ ) have small northward components at  $\sim 0904$  UT when P5 is penetrating into the plasma sheet. This means the plasma moves

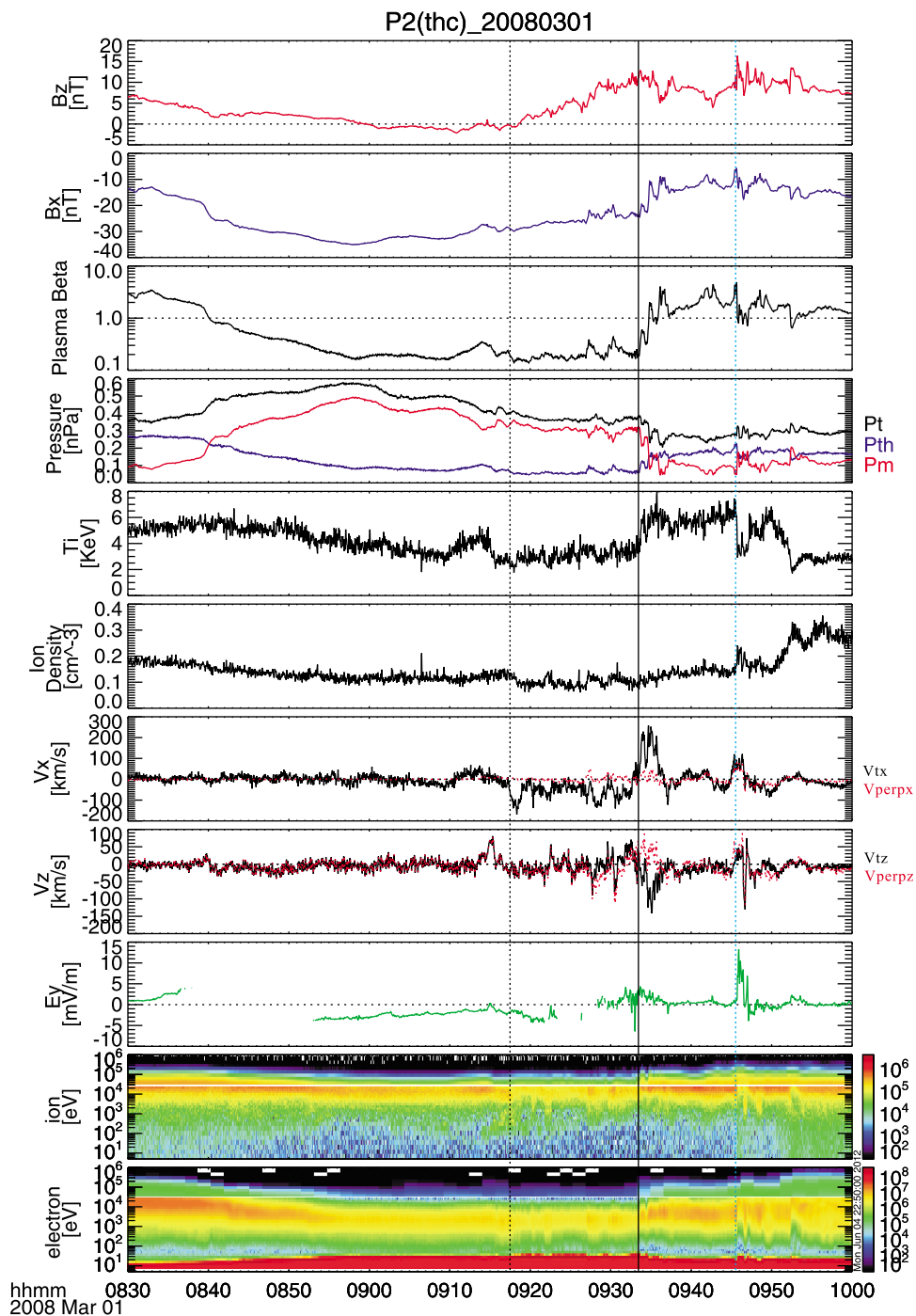


**Figure 9.** Variations of the magnetic field and plasma parameters as observed by P2 (thc) during 0830 to 1000 UT on 1 March 2008. Panel format is the same as that in Figure 6.

equatorward because P5 is located south to the neutral sheet ( $B_x < 0$ ).

[17] The second dipolarization event starts from  $\sim 0915:25$  UT (marked by cyan vertical dotted line). At this time,  $B_z$  increases again, and  $P_m$  and  $P_t$  also jump up when P5 is already in the plasma sheet. The ions have an earthward ion bulk velocity of  $\sim 280$  km/s, while  $E_y$  has a positive value of  $\sim 30$  mV/m, indicating earthward fast flows appear at this time. Ion energy flux also increases simultaneously at this moment.

[18] The third dipolarization event starts from  $\sim 0929:50$  UT (marked by cyan vertical dotted line). Similar signatures (sharp enhancements in  $B_z$  and  $P_m$ , plasma energy flux increase, large value of electric field and earthward fast flow) can also be observed at this moment as that at  $\sim 0915:25$  UT. We regard these two  $B_z$  increases in the last two events to be ‘dipolarization front’, which are very similar with those observed by *Runov et al.* [2010]. The earthward fast flows which are preceded by dipolarization fronts transfer magnetic

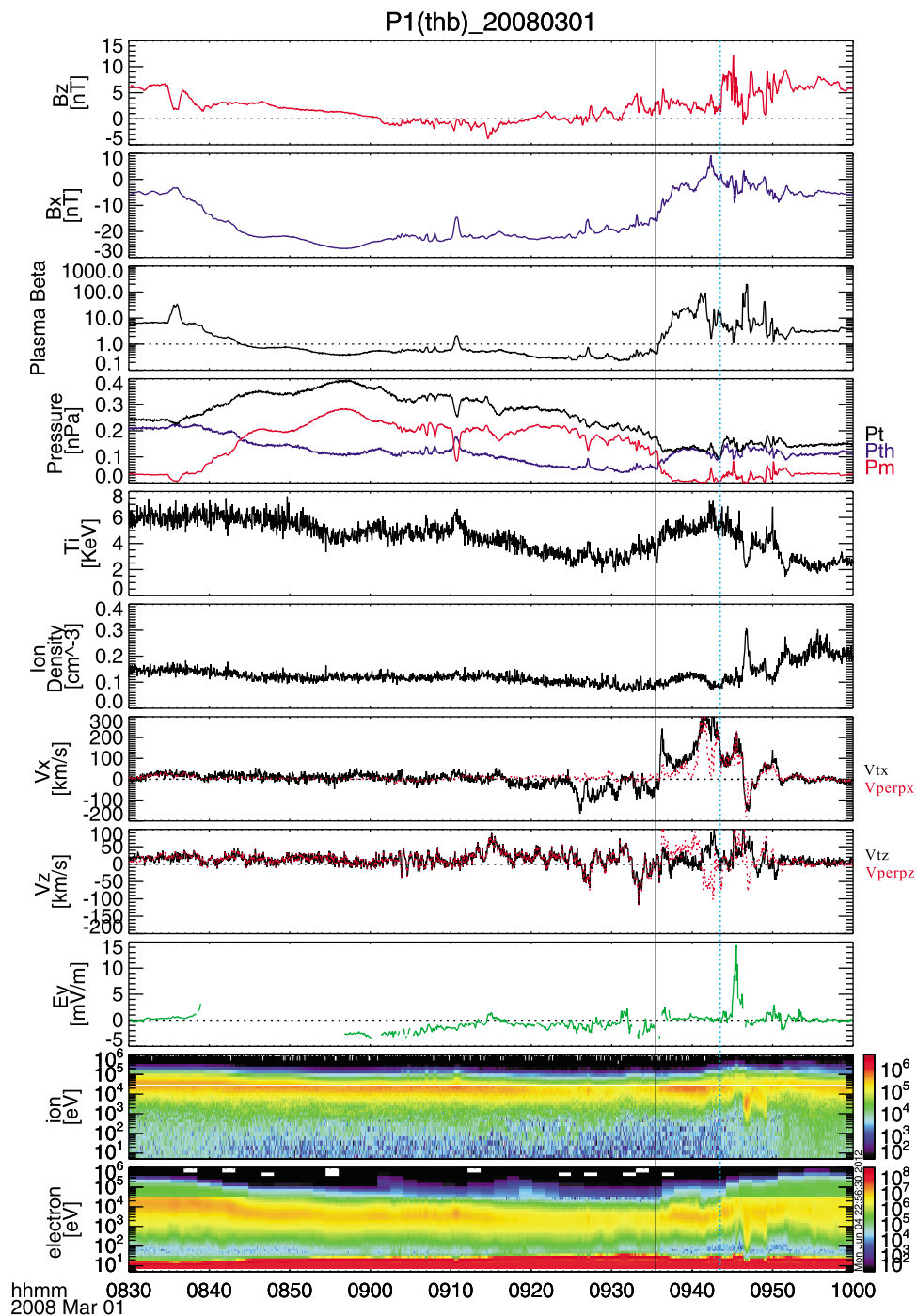


**Figure 10.** Variations of the magnetic field and plasma parameters as observed by P1 (thb) during 0830 to 1000 UT on 1 March 2008. Panel format is the same as that in Figure 6.

flux inward step by step. These earthward fast flows may originate from the activities tailward of P5 (tha).

#### 4.2. Observations at THEMIS D (P3)

[19] P3 (thd), which is tailward of P5, is located at about  $(-10.89, 1.34, -2.31)$  Re in GSM coordinates at 0900 UT. An overview of P3 observations is shown in Figure 7. At  $\sim 0858$  UT, we can see that the total pressure (Pt) starts to decrease slowly. At  $\sim 0913:54$  UT (black vertical dotted line in Figure 7), P3 has observed a sharp increase in Bz,

implying magnetic dipolarization arrival at P3. During the interval from  $\sim 0913:54$  UT to  $\sim 0918:20$  UT (black vertical solid line in Figure 7), Bz continues to increase while the other plasma moments (Pth, Pm, Pt, Ni, Ti),  $|Bx|$ , and energy flux shown keep almost unchanged. The plasma beta is continuously of a value of  $\sim 0.1$ , indicating that P3 is in the plasma sheet boundary layer in the magnetotail [Miyashita *et al.*, 2000]. The X component of ion bulk velocity (Vtx) has some small negative values during this interval. At

~0918:20 UT, Pm and Pt suddenly drop and  $|B_x|$  begins to decrease. In addition, the ion density (Ni), ion temperature (Ti) and plasma pressure (Pth) increase slightly, and the plasma (ion and electron) energy flux begins to increase. The plasma beta starts to increase at ~0918:20 UT and eventually reaches a value of  $\sim 1$ , implying that P3 enters the plasma sheet. During this process we can see that the Z component of perpendicular ion bulk flow ( $V_{\text{perpz}}$ ) is positive indicating that the plasma is moving equatorward. And the positive duskward electric field can also be detected by P3 during this process.

#### 4.3. Observations at THEMIS E (P4)

[20] P4 is at about  $(-11.13, 2.35, -2.51)$  Re in GSM coordinates at 0900 UT. It remains very close to P3  $(-10.89, 1.34, -2.31)$  Re, and their observations are very similar. Figure 8 illustrates the overviews from P4, which observes a slow total pressure (Pt) decrease at ~0857 UT as that detected at P3. As shown in Figure 8, at ~0913:42 UT (black vertical dotted line in Figure 8), a sharp increase in Bz appears, indicating the magnetic dipolarization arrival at P4. Until ~0917:20 UT (black vertical solid line in Figure 8), Ni, Ti, Pth, and the plasma energy spectrum have no large variations, and Bx, Pm and Pt show small disturbances. During the interval from ~0913:42 UT to ~0917:20 UT, the plasma beta is very low and has a value of less than 0.2. This indicates that P4 is in the PSBL during this dipolarization [Miyashita *et al.*, 2000]. During this interval, Vtx just has negative value. After ~0917:20 UT, Bz, Ni, Ti, Pth and plasma beta increase continuously, while Pm, Pt and  $|B_x|$  decrease gradually; finally, Bz becomes  $\sim 15$  nT, Bx  $\sim -20$  nT, plasma beta  $\sim 1.0$ . The plasma energy spectrum begins to increase at ~0920 UT. All these indicate that P4 is crossing the boundary layer and enters the plasma sheet since ~0917:20 UT. At ~0921 UT, P4 detects the equatorward plasma motion ( $V_{\text{perpz}} > 0$ ,  $V_z > 0$ ) and duskward electric field ( $E_y > 0$ ).

#### 4.4. Observations at THEMIS C (P2)

[21] P2 is in the mid-tail and located at  $(-14.74, 2.34, -2.81)$  Re in GSM coordinates at 0900 UT, which is tailward of P3 and P4. Figure 9 shows an overview of P2 observations. The total pressure (Pt) begins to reduce slowly at ~0858 UT. From ~0900 UT to ~0918 UT, Bz component has a negative value and it becomes northward again after ~0918 UT. Then Bz increases quasi-linearly from ~0918 UT to ~0933 UT. P2 is in the PSBL (plasma beta  $\sim 0.1-0.2$ ) during this period [Miyashita *et al.*, 2000]. We set 0918:30 UT (black vertical dotted line in Figure 9) as the dipolarization arrival at P2. From ~0918:30 UT to ~0933:20 UT (black vertical solid line in Figure 9), the plasma parameters (Pm, Pth, Ti and Ni) and Bx do not have much obvious variations, and the energy spectrum shows no significant changes. Vtx has a tailward component during this interval. However, at ~0933:20 UT,  $|B_x|$ , Pm and Pt begin to decrease sharply. Simultaneously, Pth, Ti, and energy spectrum fluxes start to increase. The plasma beta suddenly jumps from  $\sim 0.2$  to larger than 1.0. All these features mean that P2 has penetrated into the plasma sheet at this moment. At this moment,  $E_y$  has small positive values and the Z component of perpendicular ion bulk velocity ( $V_{\text{perpz}}$ ) has positive values, indicating that

the plasma is moving equatorward as P2 is located southward of neutral sheet ( $B_x < 0$ ).

[22] It is also observed that, at ~0945:30 UT (cyan vertical dotted line in Figure 9), as P2 is already in the plasma sheet, Bz has a sharp increase while Pm has a slight jump; simultaneously,  $E_y$  has a positive pulse with a value of  $\sim 13$  mV/m, and high speed earthward flows (mainly perpendicular ones) with a value of  $\sim 120$  km/s are also detected. These signatures are similar to the ones observed at ~0915:25 UT and ~0929:50 UT at P5. We may call it the dipolarization front.

#### 4.5. Observations at THEMIS B (P1)

[23] Tailward of P2 is the outermost satellite, P1, which is located at  $(-17.80, 2.39, -2.18)$  Re in GSM coordinates at 0900 UT. An overview of P1 observations is demonstrated in Figure 10. A Pt feature similar to that observed at P2, P3 and P4 has been detected. Pt begins to reduce slowly at ~0857 UT, three minutes before substorm aurora onset. We can see that, from ~0901 UT to ~0920 UT, the Bz component becomes negative, indicating that the local magnetic field is southward. After ~0920 UT, Bz grows positive with large disturbances. At ~0935:30 UT (black vertical solid line in Figure 10),  $|B_x|$ , Pm, and Pt decrease sharply. Meanwhile, Ti, Pth, and the energy spectrum fluxes increase significantly. The plasma beta jumps up quickly to around 10, implying that P1 has entered the dense plasma sheet. At this moment, we can detect equatorward plasma motions ( $V_{\text{perpz}} > 0$ ,  $B_x < 0$ ) and small duskward electric field ( $E_y > 0$ ).

[24] At ~0943:30 UT (cyan vertical dotted line in Figure 10), another Bz steep increase along with fast earthward flows (mainly perpendicular ones) and positive pulse of  $E_y$  has been detected at P1, which is very similar to those detected at P2 (~0945:30 UT) and P5 (~0915:25 UT and 0929:50 UT). It is noted that P1 has already entered the plasma sheet at this moment. We call this Bz sharp increase a dipolarization front.

### 5. Analysis and Discussions

[25] Joint observations from five THEMIS probes aligned along the tail axis near the plasma sheet during a major conjunction phase on 1 March 2008 provide us with a great opportunity to examine the global evolution of a substorm at different geocentric distances with high temporal and spatial resolution. We may now give the physical interpretations of the probe observations in Section 4.

#### 5.1. Different Types of Dipolarization

[26] Two types of dipolarization in the near-Earth magnetotail have been identified. For the first type, a "dipolarization front," there appears a sharp, large-amplitude and pulsate increase in the Z-component of the magnetic field (Bz) [Sitnov *et al.*, 2009; Runov *et al.*, 2009, 2010]. This front is associated with an earthward bursty bulk flow (BBF) in the central plasma sheet, so it is attributed to earthward magnetic flux transport [Angelopoulos *et al.*, 1994; Nakamura *et al.*, 2002; Runov *et al.*, 2009, 2010; Ge *et al.*, 2011]. For this type of dipolarization, the Bz increase is transient and pulsate, and Bz usually returns to its initial value after BBF passage [Nakamura *et al.*, 2002].

[27] The second type of dipolarization is associated with the plasma sheet expansion. *Baumjohann et al.* [1999] have used a superposed epoch approach to study the temporal evolution of this type of substorm dipolarization. It has been revealed that, such a magnetic field dipolarization moves tailward with an average velocity of 35 km/s [*Baumjohann et al.*, 1999] and this type of dipolarization can also move in the azimuthal direction [*Nagai*, 1982]. The cause of the second dipolarization is as yet undetermined. Some have suggested that it is correlated with earthward flux transport which is piled up at the near tail [*Shiokawa et al.*, 1997; *Birn et al.*, 1999]. Others, however, claim that dipolarization does not have a one-to-one relationship with braking of earthward bulk flows [*Lui et al.*, 2008; *Duan et al.*, 2011] and that near-Earth dipolarization is a non-MHD process [*Lui et al.*, 1999].

[28] In this research, when the probes are located in the PSBL, they can detect that the  $B_z$  component continues to increase and does not go back to its initial value. This type of dipolarization is the second one, as the  $B_z$  increase is not transient, and we set this dipolarization as the global one which is associated with the plasma sheet expansion. Furthermore,  $B_z$  enhances continuously while  $B_x$  remains almost constant from the arrival of global dipolarization to the beginning time of probes penetrating to the plasma sheet, implying field compression in the X direction. Some refer to this phenomenon as magnetic flux pileup [*Zhang et al.*, 2007]. So these dipolarizations may be caused by magnetic flux pileup processes. However, as there are no measurements of strong earthward fast flows when the probes are not in the plasma sheet meanwhile, this dipolarization may also be interpreted as having been caused by the CD process. When the current is disrupted, the configuration of the tail magnetic field relaxes from the tail-like shape to a more dipole-like one, indicating the global dipolarization arrives at the spacecraft location.

[29] When the probes enter into the plasma sheet in this study, they can observe another type of dipolarization, e.g., P5 at  $\sim 0915:25$  UT and  $\sim 0929:50$  UT, P2 at  $\sim 0945:30$  UT and P1 at  $\sim 0943:30$  UT. From the observations we can see that  $B_z$  has a sharp increase accompanied by fast earthward flows and it usually returns to its initial value after the fast flow-passage. So these dipolarizations belong to the first type. We call them ‘dipolarization fronts (DFs)’ just as *Sitnov et al.* [2009] and *Runov et al.* [2009, 2010]. These earthward DFs can attribute to transferring magnetic flux inward and result in the further flux pileup at the near-earth region.

## 5.2. Plasma Sheet Expansion and Its Relationship to the Global Dipolarization Arrival

[30] First we have to discuss some characteristic features of plasma sheet expansion. Plasma beta may be useful for judging different regions in the magnetotail. *Miyashita et al.* [2000] gave some definitions of the plasma beta value between plasma sheet and PSBL and between PSBL and the lobe in the north-south direction. So the large increase in plasma beta is a key feature of spacecraft penetrating into plasma sheet from PSBL or the lobe. We should note that plasma sheet expansion is not the unique cause of spacecraft penetrating into the plasma sheet from PSBL or the lobe. When spacecraft is first located in the lobe but close enough to the plasma sheet, it can cross the plasma sheet boundary

from the lobe side to the plasma sheet side during the plasma sheet expansion. However, the plasma sheet flapping motion at large or small scale can also cause the penetration into the plasma sheet from the lobe side [e.g., *Louarn et al.*, 2004]. In order to get some intrinsic features of the plasma sheet expansion, *Ohtani and Mukai* [2006] had conducted a statistical study by comparing the characteristics of lobe to plasma sheet (LB-to-PS) and plasma sheet to lobe (PS-to-LB) crossings observed by the Geotail satellite. As the flapping motion of the plasma sheet can affect statistical characteristics between the two types of crossings in the same way and the plasma sheet expansion can only be associated with the LB-to-PS crossing, *Ohtani and Mukai* [2006] then inferred the following conclusions for the plasma sheet expansion (1) the plasma moves equatorward, (2) the total pressure decreases, and (3) the local magnetic configuration becomes more dipolar. The result (1) means that the Z component of the perpendicular flow velocity is positive as the probes are always below the neutral sheet ( $B_x < 0$ ) during our substorm interval. Also *Ohtani and Mukai* [2006] suggested that the plasma moves in the opposite direction relative to the boundary motion during the plasma sheet expansion, implying that there is a finite electric field in the frame of the boundary motion and that the magnetic flux is transported from the lobe side to the plasma sheet side. This result means that it is typical for the electric field to be duskward ( $E_y > 0$ ) for the plasma sheet expansion.

[31] In this study, during the probes penetrating into the plasma sheet (the vertical solid lines in Figures 6–10), we can detect sharp drop of Pt, the more dipolar configuration of the local magnetic field ( $B_z$  increase), the equatorward motion of plasma ( $V_{\text{perpz}} > 0$ ) and the duskward electric field ( $E_y > 0$ ). All these features indicate that the penetration into the plasma sheet for this substorm is due to the plasma sheet expansion.

[32] In order to illustrate the global evolution of these dipolarizations and plasma sheet expansions, Figure 11 is presented which combines the observations of  $B_z$  and plasma beta values from all the five probes. From Figure 11, we can see that the features of plasma sheet expansions (marked by the vertical solid lines) are measured successively by P5, P4, P3, P2, and P1 at  $\sim 0904$  UT,  $\sim 0917:20$  UT,  $\sim 0918:20$  UT,  $\sim 0933:20$  UT, and  $\sim 0935:30$  UT, respectively, and the arrival times of global dipolarizations (marked by vertical dotted lines) are also successively detected by the inner four probes P5, P4, P3 and P2 at  $\sim 0900$  UT,  $\sim 0913:42$  UT,  $0913:54$  UT, and  $\sim 0918:30$  UT, respectively. We note that at each probe location (except at P1), the arrival times of the global dipolarizations are  $\sim 4$ – $15$  min earlier than the beginning time of plasma sheet expansions. So we can say that plasma sheet expansion is temporal related to the global dipolarization arrival in the magnetotail and this plasma sheet expansion can be referred to as ‘dipolarization-associated expansion’. The global dipolarizations detected by probes (in the PSBL) are the remote signatures of plasma sheet changing its configuration that may occur somewhere nearby and this plasma sheet configuration change will result in the plasma sheet expansions over the probes later. Hence, although there is a time delay between the two signatures (global dipolarization and plasma sheet expansion), these two phenomena are still caused by the same process of plasma sheet changing its configuration. In other words,

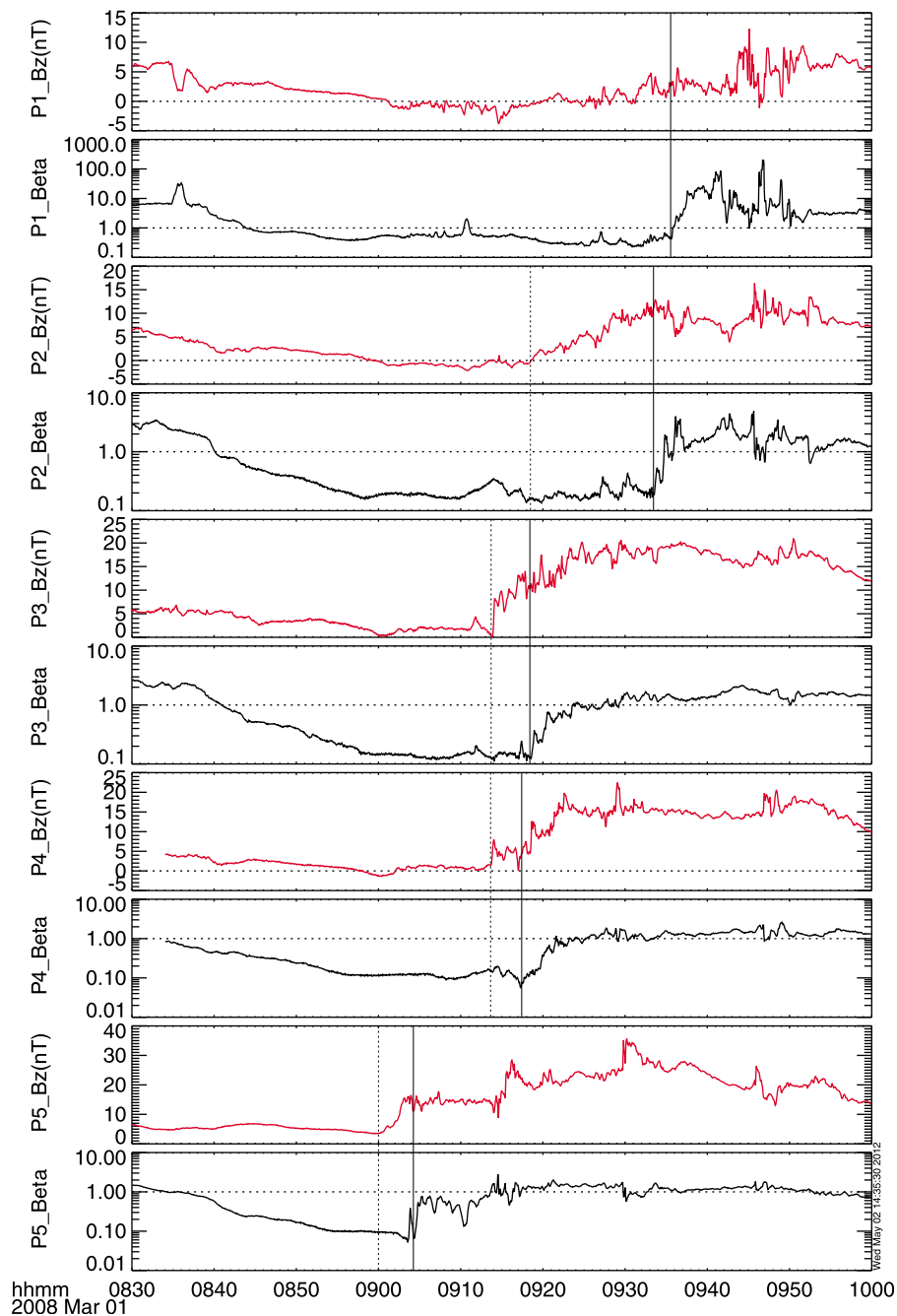


**Figure 11.** Magnetic field  $B_z$  observations from FGM and plasma beta (the ratio between plasma pressure and magnetic pressure) values onboard five THEMIS probes from 0830 to 1000 UT on 1 March 2008. The coordinate system of magnetic field used here is GSM. The vertical dotted lines indicate the global dipolarization arrival time at each probe location and the vertical solid lines indicate the beginning time of plasma sheet quick expansion.

although the plasma sheet expansion over the probe is delayed relatively to the global dipolarization signature, these two phenomena are caused by the same process but the local effects are delayed.

[33] As the plasma sheet expansion is temporal related to the global dipolarization arrival in the magnetotail and these two phenomena are caused by the same process, we assume that the global dipolarizations and the plasma sheet expansions have a very similar progression speed. So we use the

relative observation times and observation sites of multiple plasma sheet expansions to estimate progression speed and compare our result with the previous ones below. Just as shown in Figure 11, P5, P4, P3, P2 and P1 detect the feature of plasma sheet expansion at  $\sim 0904$  UT,  $\sim 0917:20$  UT,  $\sim 0918:20$  UT,  $\sim 0933:20$  UT, and  $\sim 0935:30$  UT, respectively. Timing among these probes suggests that the plasma sheet expansions have a tailward progression and also a longitudinal propagation. From Figure 1, we can see that P4,

P2 and P1 are only separated along  $x$  axis while the discrepancy between them in  $Y$  and  $Z$  axis is small. Timing between P4 and P1 indicates that the plasma sheet expansions have a tailward retreat with an average velocity of  $\sim 36$  km/s, which is consistent with the statistical results (35 km/s) of *Baumjohann et al.* [1999] but much smaller than that estimated by *Jacquey et al.* [1991] and *Ohtani et al.* [1992]. As P4 and P3 are only separated along  $y$  axis (the discrepancy between them in  $X$  and  $Z$  axis is small), the difference between the two can be caused by the expansion propagating dawnward with an average velocity of  $\sim 108$  km/s. The expansion velocity estimated from the result of *Nagai* [1982] is  $\sim 6.5^\circ/\text{min}$  duskward ( $\sim 80$  km/s) and  $\sim 2.5^\circ/\text{min}$  dawnward ( $\sim 30$  km/s) at the geosynchronous orbit of 6.6 Re. *Lopez and Lui* [1990] estimated the azimuthal expansion velocity to be  $\sim 13^\circ/\text{min}$  ( $\sim 159$  km/s assumed at the geosynchronous orbit) for their event, which was higher than *Nagai* [1982]. Recently, *Watson and Jayachandran* [2009] used ten years of GOES, POLAR and IMAGE data to study the azimuthal propagation of the dipolarizations at the geosynchronous orbit. Their result showed that the calculated azimuthal expansion speeds vary between 10 km/s and 420 km/s ( $0.8^\circ/\text{min}$  to  $34^\circ/\text{min}$ ) at the geosynchronous orbit and a large number of propagations occur in the 20 to 60 km/s ( $1.6^\circ/\text{min}$  to  $5^\circ/\text{min}$ ) range. Also *Gilson et al.* [2011] inferred the average azimuthal expansion speed of dipolarization to be  $2.2^\circ/\text{min}$  (27 km/s in the tail at geosynchronous orbit) with only a few events having expansion speeds over  $4^\circ/\text{min}$  (49 km/s) by using the longitudinal splitting of proton aurora. So the azimuthal expansion velocity in our event, which is estimated to be  $5^\circ/\text{min}$  dawnward ( $\sim 108$  km/s at  $X \sim 11$  Re), is consistent well with the results of *Nagai* [1982] and the statistical conclusion of *Watson and Jayachandran* [2009]. However, our result is a little larger than the inferred conclusion of *Gilson et al.* [2011] but much smaller than the result deduced by *Lopez and Lui* [1990].

### 5.3. Substorm Intensifications and the Multiple Dipolarizations

[34] Four increases of the THEMIS AE index (at  $\sim 0900:30$  UT,  $\sim 0908:30$  UT,  $\sim 0923:30$  UT and  $\sim 0937$  UT) are detected clearly during this substorm interval as shown in Figure 2, indicating that there are four energy release processes occurring in the magnetotail at different places. As the duration of each increase of THEMIS AE index is very short, it implies that the magnetic energy release processes in the magnetotail are short-termed and local during the substorm expansion phase. These phenomena are consistent with the scenario discussed by *Sergeev et al.* [1996]. In the coupled-mode scenario for the magnetospheric dynamics, *Sergeev et al.* [1996] suggested that the energy storage process is a global and slow quasi-static one while the energy dissipation processes are a sequence of local, sporadic, and short-termed events during both substorm and nonsubstorm times.

[35] At P1 and P2 we can detect the  $B_z$  component becomes negative from  $\sim 0901$  UT to  $\sim 0920$  UT and from  $\sim 0900$  UT to  $\sim 0919$  UT, respectively. After 0920 UT, the  $B_z$  component becomes positive again at both P1 and P2. As these energy release processes may be due to magnetic reconnection, these observations of  $B_z$  component may imply that P1 and P2 are located tailward of the first two energy release (at  $\sim 0900:30$  UT and  $\sim 0908:30$  UT) sites

and earthward of the last two energy release (at  $\sim 0923:30$  UT and  $\sim 0937$  UT) sites. As P1 and P2 are in the PSBL and not in the plasma sheet during the first two energy release processes, they could not observe fast flows rushing tailward during the first two energy release processes. However, they can observe earthward fast flows (e.g., P1 during 0936 UT to 0946 UT and P2 during 0934 UT to 0936 UT and during 0945 UT to 0947 UT) which may originate from the reconnection X line tailward of P1. When these energy release processes occur at some place in the magnetotail, the effects propagate away from the center. Then the probes inward (relative to the sites of magnetic energy releases) can detect the effects of these magnetic energy release processes later. For example, P5 can detect the effects of the second (at  $\sim 0908:30$  UT) and third (at  $\sim 0923:30$  UT) energy releases at  $\sim 0915:25$  UT and  $\sim 0929:50$  UT respectively; P1 and P2 can detect the effect of the fourth (at  $\sim 0937$  UT) energy release process at  $\sim 0943:30$  UT and  $\sim 0945:30$  UT. As the spacecraft are in the PSBL and not in the plasma sheet when the energy release processes occur in the magnetotail, we cannot confirm whether these energy release processes are magnetic reconnections or current reductions or other processes definitely in this case. Nevertheless, the plasma sheet configuration is changing its topology during the energy release process, but the spacecraft does not measure these effects locally. However, when the plasma sheet expands over the spacecraft then some of the effects can be measured. So the multiple dipolarizations detected by P5, as well as that at P2, are caused by the discrete energy release processes occurring in the magnetotail. The global dipolarizations detected at PSBL by different probes can also be caused by these discrete energy dissipation processes. So the tailward retreat of the global dipolarizations as well as the multiple plasma sheet expansions is not continuous but in stepwise sequence.

### 5.4. Test of Substorm Paradigms

[36] As the tailward progression of the global dipolarization is a shared process between NENL [e.g., *Baumjohann et al.*, 1999] and NECD [e.g., *Jacquey et al.*, 1991, 1993; *Lui*, 1996] paradigms and the observations in this case all occur after the substorm expansion onset, we cannot use this traveling sequence only to distinguish one competing model from the other clearly. However, some possible explanations should be made according to the observations. The observations of total pressure ( $P_t$ ) show that it begins to lessen at  $\sim 0857$  UT (at P1 and P4) and at  $\sim 0858$  UT (at P2 and P3), two or three minutes prior to auroral onset. This may signify that plasma sheet reconnection has already started somewhere away from the probe locations [*Miyashita et al.*, 1999, 2000]. The aurora lights up at 0900:15 UT, approximately the same time as the global dipolarization arrival at P5. As the global dipolarization may be caused by magnetic flux pileup, it indicates that the aurora breakup or substorm onset is probably in close temporal association with the flow braking and flux pileup; then,  $\sim 4$  min later, plasma sheet expansion arrives at P5. This activity expands azimuthally and tailward, so P4, P3 are engulfed first, before P2 and later P1 is reached. This scenario is consistent with the measurements in the magnetotail. In this case, we even can detect BBFs at P5 location ( $\sim 8.8$  Re) which is not

consistent with results that in most cases BBFs are braking and the flux is piled up outside  $\sim -13$  to  $-15$  Re as shown by *Shiokawa et al.* [1997].

[37] As all these observations are detected after substorm expansion onset, we cannot catch any direct measurements of either magnetic reconnection or current disruption prior to substorm onset. Although we can deduce that magnetic reconnection may have already started from the signatures of decreasing total pressure prior to substorm expansion onset, it is still not the direct conventional magnetotail reconnection observations. As the main difference between these two competing models is not detected at all due to the unsuited satellite location prior to substorm onset, thus, we still cannot declare which model observations of this substorm event (as clear as they may be) support. We need more observations in the plasma sheet before substorm onset to choose a triggering mechanism for this substorm.

## 6. Summary

[38] In this paper, we present analysis of a substorm event that occurs while five THEMIS probes are closely aligned along the tail axis. The main results of this study, based on direct multiple-point measurements, are summarized below.

[39] There are two types of dipolarization detected in this event. One is the dipolarization front which is associated with BBFs and the other is the global one which is associated with plasma sheet expansion. The global magnetic field dipolarizations are measured successively by different probes at multiple locations in the magnetotail. From the ground we can see that there are four increases of THEMIS AE index during this substorm interval. These four increases in the THEMIS AE index indicate that local, sporadic, short-term energy release processes occur close to the neutral sheet in the magnetotail during this substorm. The spacecraft can detect the effects of these energy release processes clearly in the magnetotail corresponding to each of the AE increases. For  $\sim 4$ – $15$  min after the global dipolarizations arrival, plasma sheet expansions are clearly identified at each probe. So the plasma sheet expansion is closely related to the arrival of global dipolarization and they are caused by the same processes (magnetic energy release processes) but the effects detected by the probes are delayed. The estimation of the progression of the plasma sheet expansions shows that they have a tailward leap retreat with an average velocity of  $\sim 36$  km/s. The global evolution process associated with this substorm cannot be used to choose a triggering mechanism from either the NECD or the NENL substorm model, as there is no direct measurement of either magnetic reconnection or current disruption prior to substorm expansion onset.

[40] **Acknowledgments.** This work was supported by the National Natural Science Foundation of China, grants 40974101 and 40921063, Ministry of Science and Technology of China, grant 2011CB811404, and the Specialized Research Fund for State Key Laboratories of the Chinese Academy of Sciences. We acknowledge NASA contract NAS5-02099 for use of data from the THEMIS Mission. Specifically: E. Donovan and the CSA for logistical support in fielding and data retrieval from the GBO stations and S. Mende and C. T. Russell for use of the GMAG data. The authors are also thankful to J. H. King, N. Papatashvili and CDAweb for the availability of OMNI data.

[41] Masaki Fujimoto thanks the reviewers for their assistance in evaluating this paper.

## References

- Akasofu, S. I. (1977), *Physics of Magnetospheric Substorms*, Springer, New York, doi:10.1007/978-94-010-1164-8.
- Akasofu, S.-I. (1981), Energy coupling between the solar wind and the magnetosphere, *Space Sci. Rev.*, *28*, 121–190, doi:10.1007/BF00218810.
- Angelopoulos, V. (2008), The THEMIS Mission, *Space Sci. Rev.*, *141*, 5–34, doi:10.1007/s11214-008-9336-1.
- Angelopoulos, V., W. Baumjohann, C. Kennel, F. Coroniti, M. Kivelson, R. Pellat, R. Walker, H. Lühr, and G. Paschmann (1992), Bursty bulk flows in the inner central plasma sheet, *J. Geophys. Res.*, *97*(A4), 4027–4039, doi:10.1029/91JA02701.
- Angelopoulos, V., C. F. Kennel, F. V. Coroniti, R. Pellat, M. G. Kivelson, R. J. Walker, C. T. Russell, W. Baumjohann, W. C. Feldman, and J. T. Gosling (1994), Statistical characteristics of bursty bulk flow events, *J. Geophys. Res.*, *99*(A11), 21,257–21,280, doi:10.1029/94JA01263.
- Angelopoulos, V., et al. (2008a), First results from the THEMIS mission, *Space Sci. Rev.*, *141*, 453–476, doi:10.1007/s11214-008-9378-4.
- Angelopoulos, V., et al. (2008b), Tail reconnection triggering substorm onset, *Science*, *321*, 931–935, doi:10.1126/science.1160495.
- Angelopoulos, V., et al. (2009), Response to comment on “Tail reconnection triggering substorm onset,” *Science*, *324*, 1391, doi:10.1126/science.1168045.
- Auster, H. U., et al. (2008), The THEMIS fluxgate magnetometer, *Space Sci. Rev.*, *141*, 235–264, doi:10.1007/s11214-008-9365-9.
- Baker, D. N., T. I. Pulkkinen, V. Angelopoulos, W. Baumjohann, and R. L. McPherron (1996), Neutral line model of substorms: Past result and present view, *J. Geophys. Res.*, *101*(A6), 12,975–13,010, doi:10.1029/95JA03753.
- Baumjohann, W. (2002), Modes of convection in the magnetotail, *Phys. Plasmas*, *9*(9), 3665–3667, doi:10.1063/1.1499116.
- Baumjohann, W., M. Hesse, S. Kokubun, T. Mukai, T. Nagai, and A. A. Petrukovich (1999), Substorm dipolarization and recovery, *J. Geophys. Res.*, *104*, 24,995–25,000, doi:10.1029/1999JA900282.
- Birn, J., M. Hesse, G. Haerendel, W. Baumjohann, and K. Shiokawa (1999), Flow braking and the substorm current wedge, *J. Geophys. Res.*, *104*(A9), 19,895–19,903, doi:10.1029/1999JA900173.
- Bonnell, J. W., F. S. Mozer, G. T. Delory, A. J. Hull, R. E. Ergun, C. M. Cully, V. Angelopoulos, and P. R. Harvey (2008), The Electric Field Instrument (EFI) for THEMIS, *Space Sci. Rev.*, *141*, 303–341, doi:10.1007/s11214-008-9469-2.
- Donovan, E., et al. (2006), The THEMIS all-sky imaging array-system design and initial results from the prototype imager, *J. Atmos. Sol. Terr. Phys.*, *68*(13), 1472–1487, doi:10.1016/j.jastp.2005.03.027.
- Duan, S. P., Z. X. Liu, J. Liang, Y. C. Zhang, and T. Chen (2011), Multiple magnetic dipolarizations observed by THEMIS during a substorm, *Ann. Geophys.*, *29*, 331–339, doi:10.5194/angeo-29-331-2011.
- Dungey, J. W. (1961), Interplanetary magnetic field and auroral zones, *Phys. Rev. Lett.*, *6*(2), 47–48, doi:10.1103/PhysRevLett.6.47.
- Frey, S., V. Angelopoulos, M. Bester, J. Bonnell, T. Phan, and D. Rummel (2008), Orbit design for the THEMIS mission, *Space Sci. Rev.*, *141*, 61–89, doi:10.1007/s11214-008-9441-1.
- Ge, Y. S., J. Raeder, V. Angelopoulos, M. L. Gilson, and A. Runov (2011), Interaction of dipolarization fronts within multiple bursty bulk flows in global MHD simulations of a substorm on 27 February 2009, *J. Geophys. Res.*, *116*, A00123, doi:10.1029/2010JA015758.
- Gilson, M. L., J. Raeder, E. Donovan, Y. S. Ge, and S. B. Mende (2011), Statistics of the longitudinal splitting of proton aurora during substorms, *J. Geophys. Res.*, *116*, A08226, doi:10.1029/2011JA016640.
- Gonzalez, W. D. (1990), A unified view of solar wind-magnetosphere coupling functions, *Planet. Space Sci.*, *38*, 627–632, doi:10.1016/0032-0633(90)90068-2.
- Harris, S. E., et al. (2008), THEMIS ground based observatory system design, *Space Sci. Rev.*, *141*, 213–233, doi:10.1007/s11214-007-9294-z.
- Hones, E. W., Jr., T. Pytte, and H. I. West Jr. (1984), Associations of geomagnetic activity with plasma sheet thinning and expansion: A statistical study, *J. Geophys. Res.*, *89*, 5471–5478, doi:10.1029/JA089IA07p05471.
- Hsu, T.-S., and R. L. McPherron (2003), Occurrence frequencies of IMF triggered and nontriggered substorms, *J. Geophys. Res.*, *108*(A7), 1307, doi:10.1029/2002JA009442.
- Jacquey, C., J. A. Sauvaud, and J. Dandouras (1991), Location and propagation of the magnetotail current disruption during substorm expansion: Analysis and simulation of an ISEE multi-onset event, *Geophys. Res. Lett.*, *18*(3), 389–392, doi:10.1029/90GL02789.
- Jacquey, C., J. A. Sauvaud, I. Dandouras, and A. Korth (1993), Tailward propagating cross-tail current disruption and dynamics of near-Earth tail: A multi-point measurement analysis, *Geophys. Res. Lett.*, *20*, 983–986, doi:10.1029/93GL00072.
- Liu, J., C. Gabrielse, V. Angelopoulos, N. A. Friswell, L. R. Lyons, J. P. McFadden, J. Bonnell, and K. H. Glassmeier (2011), Superposed epoch

- analysis of magnetotail flux transport during substorms observed by THEMIS, *J. Geophys. Res.*, *116*, A00I29, doi:10.1029/2010JA015886.
- Lopez, R. E., and A. T. Y. Lui (1990), A multisatellite case study of the expansion of a substorm current wedge in the near-Earth magnetotail, *J. Geophys. Res.*, *95*(A6), 8009–8017, doi:10.1029/JA095iA06p08009.
- Louarn, P., G. Fruit, E. Budnik, J. A. Sauvaud, C. Jacquey, D. Le Quéau, H. Rème, E. Lucek, and A. Balogh (2004), On the propagation of low-frequency fluctuations in the plasma sheet: 1. Cluster observations and magnetohydrodynamic analysis, *J. Geophys. Res.*, *109*, A03216, doi:10.1029/2003JA010228.
- Lu, G., et al. (1998), Global energy deposition during the January 1997 magnetic cloud event, *J. Geophys. Res.*, *103*, 11,685–11,694, doi:10.1029/98JA00897.
- Lui, A. T. Y. (1996), Current disruption in the Earth's magnetosphere: Observations and models, *J. Geophys. Res.*, *101*(A6), 13,067–13,088, doi:10.1029/96JA00079.
- Lui, A. T. Y. (2009), Comment on "Tail reconnection triggering substorm onset," *Science*, *324*, 1391, doi:10.1026/science.1167726.
- Lui, A. T. Y., R. E. Lopez, B. J. Anderson, K. Takahashi, L. J. Zanetti, R. W. McEntire, T. A. Potemra, D. M. Klumpar, E. M. Greene, and R. Strangeway (1992), Current disruptions in the near-Earth neutral sheet region, *J. Geophys. Res.*, *97*, 1461–1480, doi:10.1029/91JA02401.
- Lui, A. T. Y., K. Liou, M. Nosé, S. Ohtani, D. J. Williams, T. Mukai, K. Tsuruda, and S. Kokubun (1999), Near-Earth dipolarization: Evidence for a non-MHD process, *Geophys. Res. Lett.*, *26*(19), 2905–2908, doi:10.1029/1999GL003620.
- Lui, A. T. Y., et al. (2007), Prelude to THEMIS tail conjunction, *Ann. Geophys.*, *25*, 1001–1009, doi:10.5194/angeo-25-1001-2007.
- Lui, A. T. Y., et al. (2008), Determination of the substorm initiation region from a major conjunction interval of THEMIS satellites, *J. Geophys. Res.*, *113*, A00C04, doi:10.1029/2008JA013424.
- Lyons, L. R. (1995), A new theory for magnetospheric substorms, *J. Geophys. Res.*, *100*(A10), 19,069–19,081, doi:10.1029/95JA01344.
- Lyons, L. R. (1996), Substorms: Fundamental observation features, distinction from other disturbances, and external triggering, *J. Geophys. Res.*, *101*(A6), 13,011–13,025, doi:10.1029/95JA01987.
- Lyons, L. R., G. T. Blanchard, J. C. Samson, R. P. Lepping, T. Yamamoto, and T. Moretto (1997), Coordinated observations demonstrating external substorm triggering, *J. Geophys. Res.*, *102*(A12), 27,039–27,051, doi:10.1029/97JA02639.
- McFadden, J. P., C. W. Carlson, D. Larson, M. Ludlam, R. Abiad, B. Elliott, P. Turin, M. Marckwordt, and V. Angelopoulos (2008a), The THEMIS ESA plasma instrument and in-flight calibration, *Space Sci. Rev.*, *141*, 277–302, doi:10.1007/s11214-008-9440-2.
- McFadden, J. P., C. W. Carlson, D. Larson, J. Bonnell, F. Mozer, V. Angelopoulos, K.-H. Glassmeier, and U. Auster (2008b), THEMIS ESA first science results and performance issues, *Space Sci. Rev.*, *141*, 477–508, doi:10.1007/s11214-008-9433-1.
- McPherron, R. L. (1979), Magnetospheric substorms, *Rev. Geophys.*, *17*(4), 657–681, doi:10.1029/RG017i004p00657.
- McPherron, R. L. (1991), Physical processes producing magnetospheric substorms and magnetic storms, in *Geomagnetism*, vol. 4, edited by J. Jacobs, pp. 593–739, Academic, London.
- Mende, S. B., S. E. Harris, H. U. Frey, V. Angelopoulos, C. T. Russell, E. Donovan, B. Jackel, M. Greffen, and L. M. Peticolas (2008), The THEMIS array of ground-based observatories for the study of auroral substorms, *Space Sci. Rev.*, *141*, 357–387, doi:10.1007/s11214-008-9380-x.
- Miyashita, Y., S. Machida, A. Nishida, T. Mukai, Y. Saito, and S. Kokubun (1999), GEOTAIL observations of total pressure and electric field variations in the near and mid-distant tail associated with substorm onsets, *Geophys. Res. Lett.*, *26*(6), 639–642, doi:10.1029/1999GL900031.
- Miyashita, Y., S. Machida, T. Mukai, Y. Saito, K. Tsuruda, H. Hayakawa, and P. R. Sutcliffe (2000), A statistical study of variations in the near and mid-distant magnetotail associated with substorm onsets: GEOTAIL observations, *J. Geophys. Res.*, *105*(A7), 15,913–15,930, doi:10.1029/1999JA000392.
- Nagai, T. (1982), Observed magnetic substorm signatures at synchronous altitude, *J. Geophys. Res.*, *87*, 4405–4417, doi:10.1029/JA087iA06p04405.
- Nakamura, R., et al. (2002), Motion of the dipolarization front during a flow burst event observed by Cluster, *Geophys. Res. Lett.*, *29*(20), 1942, doi:10.1029/2002GL015763.
- Ohtani, S., and T. Mukai (2006), Plasma sheet expansion: Statistical characteristics, *J. Geophys. Res.*, *111*, A05206, doi:10.1029/2005JA011547.
- Ohtani, S., S. Kokubun, and C. Russell (1992), Radial expansion of the tail current disruption during substorms: A new approach to the substorm onset region, *J. Geophys. Res.*, *97*(A3), 3129–3136, doi:10.1029/91JA02470.
- Pu, Z. Y., et al. (1999), Ballooning instability in the presence of a plasma flow: A synthesis of tail reconnection and current disruption models for the initiation of substorms, *J. Geophys. Res.*, *104*, 10,235–10,248, doi:10.1029/1998JA900104.
- Pu, Z. Y., A. Korth, Z. X. Chen, Z. X. Liu, S. Y. Fu, G. Zong, M. H. Hong, and X. M. Wang (2001), A global synthesis model of dipolarization at substorm expansion onset, *J. Atmos. Sol. Terr. Phys.*, *63*, 671–681, doi:10.1016/S1364-6826(00)00183-8.
- Roux, A., O. Le Contel, C. Coillot, A. Bouabdellah, B. de la Porte, D. Alison, S. Ruocco, and M. C. Vassal (2008), The Search Coil Magnetometer for THEMIS, *Space Sci. Rev.*, *141*, 265–275, doi:10.1007/s11214-008-9455-8.
- Runov, A., et al. (2008), Multipoint in situ and ground-based observations during auroral intensifications, *J. Geophys. Res.*, *113*, A00C07, doi:10.1029/2008JA013493.
- Runov, A., V. Angelopoulos, M. I. Sitnov, V. A. Sergeev, J. Bonnell, J. P. McFadden, D. Larson, K. Glassmeier, and U. Auster (2009), THEMIS observations of an earthward-propagating dipolarization front, *Geophys. Res. Lett.*, *36*, L14106, doi:10.1029/2009GL038980.
- Runov, A., et al. (2010), Dipolarization fronts in the magnetotail plasma sheet, *Planet. Space Sci.*, *59*, 517–525, doi:10.1016/j.pss.2010.06.006.
- Russell, C. T., P. J. Chi, D. J. Dearborn, Y. S. Ge, B. Kuo-Tiong, J. D. Means, D. R. Pierce, K. M. Rowe, and R. C. Snare (2008), THEMIS ground-based magnetometers, *Space Sci. Rev.*, *141*(1–4), 389–412, doi:10.1007/s11214-008-9337-0.
- Saito, M. H., D. Fairfield, G. Le, L.-N. Hau, V. Angelopoulos, J. P. McFadden, U. Auster, J. W. Bonnell, and D. Larson (2011), Structure, force balance, and evolution of incompressible cross-tail current sheet thinning, *J. Geophys. Res.*, *116*, A10217, doi:10.1029/2011JA016654.
- Sergeev, V. A., T. I. Pulkkinen, and R. J. Pellinen (1996), Coupled-mode scenario for the magnetospheric dynamics, *J. Geophys. Res.*, *101*(A6), 13,047–13,065, doi:10.1029/95JA03192.
- Shen, C., Z. Liu, and T. Kamei (2002), A physics-based study of the *Dst*-*AL* relationship, *J. Geophys. Res.*, *107*(A1), 1009, doi:10.1029/2001JA900121.
- Shiokawa, K., W. Baumjohann, and G. Haerendel (1997), Braking of high speed flows in the near-Earth tail, *Geophys. Res. Lett.*, *24*(10), 1179–1182, doi:10.1029/97GL01062.
- Shiokawa, K., et al. (1998), High-speed ion flow, substorm current wedge, and multiple Pi 2 pulsations, *J. Geophys. Res.*, *103*, 4491–4507, doi:10.1029/97JA01680.
- Sitnov, M. I., M. Swisdak, and A. V. Divin (2009), Dipolarization fronts as a signature of transient reconnection in the magnetotail, *J. Geophys. Res.*, *114*, A04202, doi:10.1029/2008JA013980.
- Tsyganenko, N. A. (1996), Effects of the solar wind conditions on the global magnetospheric configuration as deduced from data-based field models, in *Proceedings of the Third International Conference on Substorms (ICS-3), Versailles, France, 12–17 May 1996*, edited by E. Rolfe and B. Kaldeich, *Eur. Space Agency Spec. Publ.*, *ESA SP-389*, 181–185.
- Watson, C. J., and P. T. Jayachandran (2009), Azimuthal expansion of the dipolarization at geosynchronous orbits associated with substorms, *Ann. Geophys.*, *27*, 1113–1118, doi:10.5194/angeo-27-1113-2009.
- Zhang, H., et al. (2007), TC-1 observations of flux pileup and depolarization-associated expansion in the near-Earth magnetotail during substorms, *Geophys. Res. Lett.*, *34*, L03104, doi:10.1029/2006GL028326.